ORIGINAL PAPER

Analytic signal space partitioning and symbolic dynamic filtering for degradation monitoring of electric motors

Subhadeep Chakraborty · Asok Ray · Aparna Subbu · Eric Keller

Abstract This study presents an application of the recently reported theories of analytic signal space partitioning (ASSP) and symbolic dynamic filtering (SDF) to address degradation monitoring in permanent magnet synchronous motors (PMSM). An (experimentally validated) mathematical model of generic PMSM is chosen to monitor degradation/fault events on a simulation test bed; and the estimated parameter of health condition is observed to vary smoothly and monotonically with degradation in magnetization of the PMSM.

Keywords Hilbert transform · Symbolic dynamic filtering · Fault diagnosis · Electric motors

1 Introduction

Recent literature has reported theoretical aspects of analytic signal space partitioning (ASSP) [1] and symbolic dynamic filtering (SDF) [2,3] for anomaly detection in dynamical systems. This study presents the degradation monitoring in permanent magnet synchronous motors (PMSM) as an application of ASSP and SDF. The resulting algorithm computes a health indicator based on the time-series data, generated from an (experimentally validated) mathematical model of generic

S. Chakraborty · A. Ray (✉) · A. Subbu · E. Keller
The Pennsylvania State University, University Park, USA
e-mail: axr2@psu.edu

S. Chakraborty
e-mail: szc138@psu.edu

A. Subbu
e-mail: avs127@psu.edu

E. Keller
e-mail: eek105@psu.edu

PMSM [4] on a simulation test bed. The estimated (scalar) parameter of motor health condition increases smoothly and monotonically as the degradation in the permanent magnet component of the motor progresses.

The underlying theories of ASSP and SDF are briefly described in Sect. 2. The PMSM model is presented in Sect. 3 along with the analysis of its failure modes. The simulation results are presented in Sect. 4 for gradually evolving faults. Finally, the paper is summarized and concluded in Sect. 5 with the recommendations for future research.

2 Review of underlying mathematical concepts

Although the theories of ASSP and SDF are described in detail in previous publications [1–3], this section briefly presents the underlying concepts for completeness of this paper.

2.1 Analytic signal space partitioning

Analytic signal space partitioning (ASSP) of time-series data is used for symbol sequence generation that is an essential ingredient of SDF.

Hilbert transform [5] of a real-valued signal $x(t)$ is defined as:

$$\widetilde{x}(t) = \mathcal{H}[x](t) = \frac{1}{\pi} \int_{\mathbb{R}} \frac{x(\tau)}{t - \tau} \mathrm{d}\tau \qquad (1)$$

that is, $\widetilde{x}(t)$ is the convolution of $x(t)$ with $\frac{1}{\pi t}$ over the real field $\mathbb{R}$, which is represented in the Fourier domain as:

$$\mathcal{F}[\widetilde{x}](\xi) = -i\, sgn(\xi)\, \mathcal{F}[x](\xi) \qquad (2)$$

where $sgn(\xi) = \begin{cases} +1 & \text{if } \xi > 0 \\ -1 & \text{if } \xi < 0 \end{cases}$

The corresponding complex-valued analytic signal is defined as:

$$\mathcal{A}[x](t) = x(t) + i \, \widetilde{x}(t) \tag{3}$$

$$\mathcal{A}[x](t) = A(t) \exp\left(i \, \varphi(t)\right) \tag{4}$$

where $A(t)$ and $\varphi(t)$ are called the instantaneous amplitude and instantaneous phase of $\mathcal{A}[x](t)$, respectively.

Given a set of real-valued time-series data, Hilbert transform of this data set yields a pseudo-phase plot, that is, constructed from the analytic signal by a bijective mapping of the complex domain onto the $\mathbb{R}^2$, i.e., by plotting the real and the imaginary parts of the analytic signal on the x and y axes, respectively. The time-dependent analytic signal in Eq. (3) is now represented as a (one-dimensional) trajectory in the the two-dimensional pseudo-phase space.

Let Ξ be a compact region in the pseudo-phase space, which encloses the trajectory. The objective here is to partition Ξ into finitely many mutually exclusive and exhaustive segments, where each segment is labeled with a symbol or letter. The segments are determined by magnitude and phase of the analytic signal and also from the density of data points in these segments; that is, if the magnitude and phase of a data point of the analytic signal lies within a segment or on its boundary, then that data point is labeled with the corresponding symbol. This process of symbol generation is called ASSP [1] and the resulting set of (finitely many) symbols is called the alphabet Σ.

One possible way of partitioning Ξ is to divide the magnitude and phase of the time-dependent analytic signal in Eq. (3) into uniformly spaced segments between their minimum and maximum values. This is called uniform partitioning. An alternative method, known as maximum entropy partitioning [6], maximizes the entropy of the partition, which imposes a uniform probability distribution on the symbols. In this partitioning, parts of the state space with rich information are partitioned into finer segments than those with sparse information. The ASSP algorithm makes use of either one or both of these partitioning methods.

2.2 symbolic dynamic filtering

Given a representative symbol sequence derived from the real-valued time series, the concept of D-Markov Machine [2,3] has been adopted for degradation monitoring of the PMSM system under consideration. The D-Markov machine has a state–space structure where the states of the machine are represented by blocks $\sigma_i \sigma_{i+1} \sigma_{i+2} \ldots \sigma_{i+D-1}$ in the symbol sequence. Thus, with cardinality $|\Sigma|$ of the alphabet and depth D of a symbol string of a state, the total maximum number of states in the D-Markov machine is given by $|\Sigma|^D$. Thus, the state machine moves from one state to another upon occurrence of a symbol. All symbol sequences that have the
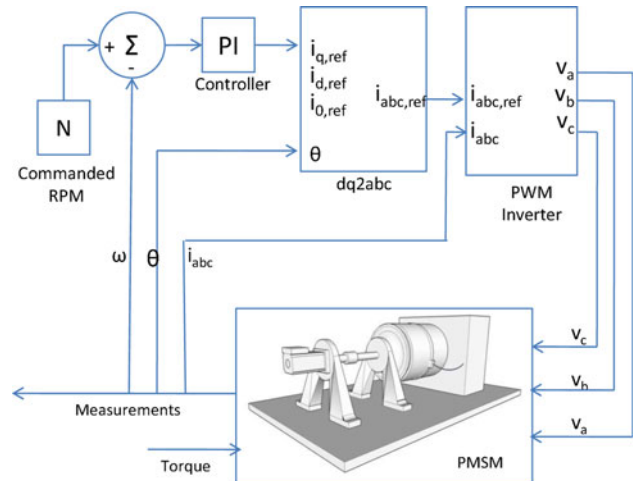
Fig. 1 Inverter-driven permanent magnet synchronous motor (PMSM) system

same last D symbols represent the same state. In the absence of any degradation in the PMSM system, there should be no change in the statistics of the symbol sequence, which implies that the states of the D-Markov machine at different time epochs should have identical probability distribution. A change in the dynamics may cause deviation of the probability distribution of the states. One possible measure of this deviation, which is called the anomaly measure, is the angle between the state probability vectors at the nominal and off-nominal conditions. The anomaly measure at the kth epoch is defined as:

$$\mu_k = \arccos\left(\frac{\langle p_0, p_k \rangle}{\|p_0\|_2 \, \|p_k\|_2}\right) \tag{5}$$

where $\langle p_0, p_k \rangle$ is the inner product of probability vectors p_0 and p_k at the nominal condition and the kth epoch, respectively; and $\| \bullet \|_2$ is the Euclidian norm of $\bullet$.

3 Description of the simulation test bed

This section describes the simulation test bed, which is a representation of an inverter-driven permanent magnet synchronous motor (PMSM) [4], as depicted in Fig. 1. The simulation model of a generic $PMSM$, without a damper winding, is similar to that of a wound-rotor synchronous machine under the following simplifying assumptions:

- negligible magnetic field saturation;
- negligible eddy current loss and hysteresis loss;
- negligible field current dynamics;
- sinusoidal-induced electromotive force.

In rotor reference frame, the governing equations of the stator voltage are given as:

$$v_q = Ri_q + \frac{d\lambda_q}{dt} + \omega_s\lambda_d \tag{6}$$

$$v_d = Ri_d + \frac{d\lambda_d}{dt} - \omega_s\lambda_q \tag{7}$$

where the subscripts q and d have their usual significance of quadrature and direct axes in the equivalent 2-phase representation; and

$$\lambda_q = L_q i_q \quad \text{and} \quad \lambda_d = L_d i_d + \lambda_{af} \tag{8}$$

with v, i, and L being the corresponding axis voltages, stator currents and inductances; R and ω_s are the stator resistance and inverter frequency, respectively, while λ_{af} is the flux linkage of the rotor magnets with the stator.

The generated electromagnetic torque is expressed as:

$$T_e = 1.5P\left[\lambda_{af}i_q + (L_d - L_q)i_d i_q\right] \tag{9}$$

and the equation of motor dynamics is given by:

$$T_e = T_L + B\omega_r + J\frac{d\omega_r}{dt} \tag{10}$$

where P is the number of pole pairs, T_L is the load torque, B is the damping coefficient, ω_r is the rotor speed, and J is the moment of inertia. The rotor speed $\omega_r = \omega_s/P$.

In state–space setting, the governing equations of the *PMSM* take the following form:

$$\frac{di_q}{dt} = \left(v_q - Ri_q - \omega_s L_d i_d - \omega_s\lambda_{af}\right)/L_q \tag{11}$$

$$\frac{di_d}{dt} = \left(v_d - Ri_d + \omega_s L_q i_q\right)/L_d \tag{12}$$

$$\frac{d\omega_r}{dt} = (T_e - T_L - B\omega_r)/J \tag{13}$$

In the control scheme shown in Fig. 1, i_d is forced to be zero. Consequently,

$$\lambda_d = \lambda_{af} \quad \text{and} \quad T_e = 1.5P\lambda_{af}i_q \tag{14}$$

In the above equation, the torque T_e is proportional to the quadrature axis current, because the magnetic flux linkage λ_{af} is constant.

In the simulation test bed, the motor model is a three-phase four-pole device rated at 1.1 kW, 220 V, 3000 rpm and is fed by a pulse-width-modulated (PWM) inverter. The stator resistance of the motor is $R_s = 0.05\ \Omega$; the quadrature-axis- and direct-axis inductances are $L_q = L_d = 6.35 \times 10^{-4} H$, the nominal flux linkage $\lambda_{af} = 0.192$ Wb, the rotor inertia $J = 0.011$ kg m^2, and the friction factor is $B = 0.001889$ kg m^2 s.

A simple hysteresis current controller has been employed for controlling the power circuit that drives the PMSM, as seen in Fig. 1. Two control loops have been employed. The inner loop regulates the motor's stator currents, whereas the outer loop uses a proportional-integral controller to regulate the motor's speed. In this control scheme, the line currents, i_a, i_b, and i_c are measured. The reference values are compared with the actual values of the currents, and the error signal, thus constructed is used for generating the gate turn on/off commands. In the present scenario, a hysteresis band of $0.25A$ on either side of the reference current i is employed.

Fig. 2 Demagnetization property of neodymium–iron–boron (Nd–Fe–B) [7]

4 Failure modes and results

Failures due to demagnetization of the permanent magnet in both surface-mounted and buried-magnet PMSMs have been widely studied in literature [7]. Demagnetization may occur due to several reasons, notable among which are those due to a strong opposing magnetic field, and also due to high temperature. A strong opposing magnetic flux is created in the event of a short circuit between a machine terminal and the (normally) isolated neutral point of the machine. A short circuit between two or three terminals of the machine and a short circuit in one of the diodes or electronic valves of the inverter give rise to a direct current (DC) in the machine.

The risk of irreversible demagnetization is present, when the counter-acting flux lowers the flux density in the magnet to a point (H_D, B_D) in Fig. 2, which is just above the so-called critical knee of the magnet's BH-curve. A common method to check the demagnetization of the permanent magnets due to armature reaction is described in [8] under the restrictive assumption that the permanent magnet pole has uniform saturation. A more accurate way to check the demagnetization is with the finite element method. Partial or complete demagnetization may also result from high temperature of the magnets and the winding insulation. The temperature increases the resistance of the winding wires and the increased resistance affects the applied current to the motor.
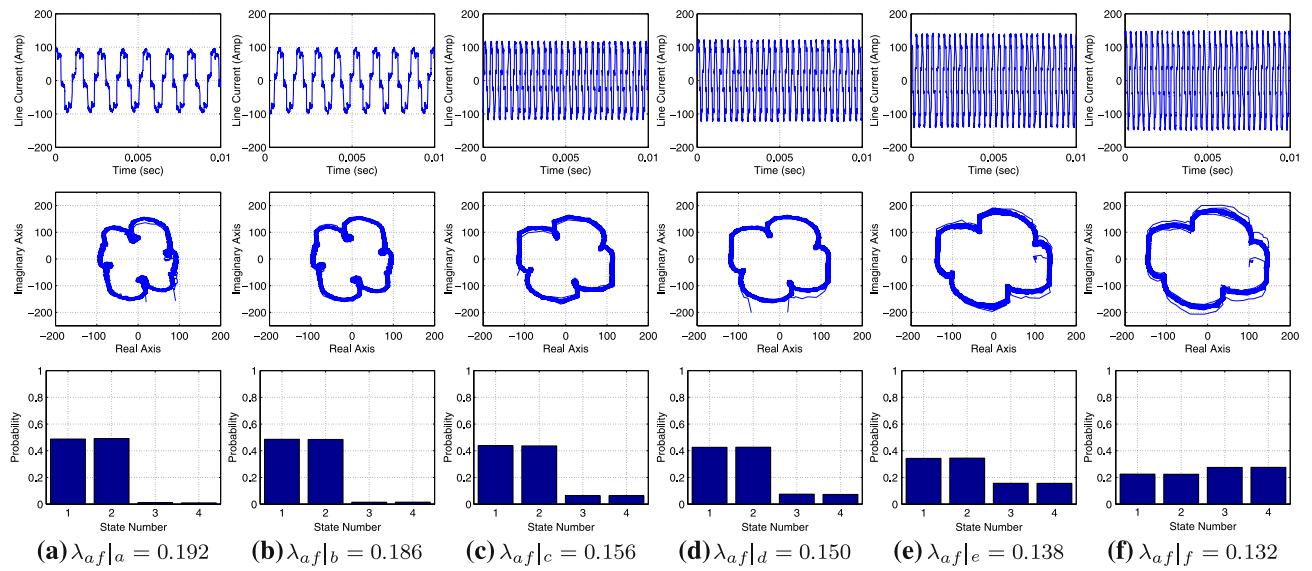
Fig. 3 Rows from *top* to *bottom*: 1 Line current i_a; 2 analytic signal derived from time series; and 3 pattern vectors derived from the *D*-Markov machine

At higher temperatures ($\sim$100°C), an appreciable deterioration in acceleration might be noticed, since the torque generated by a reduced magnetic flux drops below its nominal value.

In this paper, health monitoring of PMSM is proposed by SDF [2,3] in conjunction with the ASSP [1] that are briefly described in Sect. 2. The inverter-driven PMSM in Fig. 1 is assumed to undergo a steady deterioration in terms of permanent magnet flux linkage λ_{af} that drops from its nominal value of 0.192 to 0.007 Wb. The current signals i_a, i_b, and i_c (that are contaminated by additive zero-mean Gaussian noise $\sim$ **N**(0, 10)) are collected from the motor output at several partially demagnetized conditions of the rotor.

Collected data of the line current i_a are Hilbert transformed in the form of analytic signals for conversion into discrete symbols as described in Sect. 2. The top row of Fig. 3 shows the time series of line current i_a for six different demagnetized conditions of the rotor magnets, followed by the analytic signal corresponding to each time-series data in the next row. Maximum entropy partitioning is employed in the radial direction, while the data are uniformly partitioned in the angular direction. The partitioning procedure has been discussed in Sect. 2 and in greater detail in previous publications [1–3,6]. In this paper, an alphabet size of $|\Sigma| = 4$ and a depth of $D = 1$ has been employed. Based on the observed data sets, this choice of $|\Sigma|$ was made as a trade-off between anomaly detection capability and robustness to measurement noise. The pattern vector obtained by constructing the *D*-Markov machine representation of the motor characterizes the health condition of the motor in general. The state probability vectors are shown in the bottom
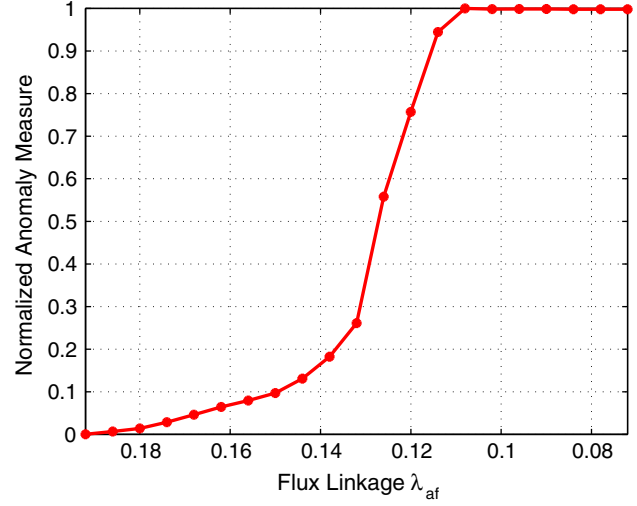
Fig. 4 Anomaly measure in a permanent magnet synchronous motor

row in Fig. 3. This visualization shows how the structure of the underlying distribution changes as the fault progresses.

The behavior pattern of the motor at its nominal operating condition depicted in the three plates in Fig. 3a; and the corresponding plates in Fig. 3b show an incipient fault condition at a very early stage of its growth, where the flux linkage has only deteriorated by $\Delta\lambda_{af}|_{a-b} = \lambda_{af}|_b - \lambda_{af}|_a = -0.006$. In contrast, when the motor fault is in an advanced stage, a significant change in behavior pattern occurs for a small incremental damage (represented by the motor flux linkage condition) as seen in Fig. 3e and f, where $\Delta\lambda_{af}|_{(e-f)} = \lambda_{af}|_f - \lambda_{af}|_e = -0.006$. In this damaged condition of the

motor, the degradation monitoring filter ensures a relatively significant change in the pattern vector, ensuring a sensitive and robust fault detection. The plates in Fig. 3c and d show two intermediate fault conditions.

The angle measure in Eq. (5) has been used to quantify the departure of the motor behavior from its nominal operating condition. The information on gradual degradation of the PMSM is assimilated in form of a profile of normalized anomaly measure μ versus the slowly changing parameter of permanent magnet flux linkage λ_{af}, as seen in Fig. 4. The small positive slope of the anomaly measure curve at incipient fault conditions (e.g., $\lambda_{af} \approx 0.18$) is highly desirable from the perspective of suppressing undesirable false alarms when the PMSM is in a healthy condition. On the other hand, at a near-critical condition (e.g., $\lambda_{af} \approx 0.14$), the large curvature of the anomaly measure curve guarantees high sensitivity to small degradation, which reduces the probability of missed detection when the PMSM is at an advanced stage of degradation. Finally, flattening out of the anomaly measure curve after λ_{af} drops at or below the threshold value of $\lambda_{af} \approx 0.11$ indicates that PMSM is practically inoperable hereafter.

5 Summary, conclusions, and future research

This study presents a data-driven method for degradation monitoring of PMSM that are extensively used in both commercial and military aircraft. The degradation monitoring algorithm is built upon the theories of ASSP [1] and SDF [2,3]. The degradation monitoring algorithm has been tested on time-series data, collected from an (experimentally validated) simulation model of a generic PMSM.

This paper presents an application of the recently reported theories of ASSP and SDF, where it is concluded that their combination is potentially a useful tool for detecting incipient faults in electric motors such as PMSM. However, further theoretical, computational, and experimental research is necessary before the proposed degradation monitoring technique can be considered for incorporation into the Instrumentation and Control system of commercial-scale plants using electric motors. Validation of the degradation monitoring algorithm on an experimental test bed has been planned based on the findings of the simulation results; and the experimental test bed is being developed.

References

1. Subbu, A., Ray, A.: Space partitioning via Hilbert transform for symbolic time series analysis. Appl. Phys. Lett. **92**(8), 084107–1 to 084107–3 (2008)
2. Ray, A.: Symbolic dynamic analysis of complex systems for anomaly detection. Signal Process. **84**(7), 1115–1130 (2004)
3. Rao, C., Ray, A., Sarkar, S., Yasar, M.: Review and comparative evaluation of symbolic dynamic filtering for detection of anomaly patterns. Signal Image Video Process. (2008). doi:10.1007/s11760-008-0061-8
4. Pillay, P., Krishnan, R.: Modeling, simulation, and analysis of permanent-magnet motor drives, Part I: The permanent-magnet synchronous motor drive. IEEE Trans Ind Appl **25**(2), 265–273 (1989)
5. Cohen, L.: Time-frequency analysis. Prentice Hall PTR, Upper Saddle River (1995)
6. Rajagopalan, V., Ray, A.: Symbolic time series analysis via wavelet-based partitioning. Signal Process. **86**(11), 3309–3320 (2006)
7. Thelin, P.: Short circuit fault conditions of a buried PMSM investigated with FEM. In: NORPIE/2002, Stockholm, Sweden (2002)
8. Hendershot, J., Miller, T.: Design of Brushless Permanent-Magnet Motors. Oxford University Press, Oxford (1996)